



Single-Atomic Dispersion of Fe and Co Supported on Reduced Graphene Oxide for High-Performance Lithium–Sulfur Batteries

Sajad Rahimi, Lorenzo Stievano, Laetitia Dubau, Cristina Iojoiu, Lauréline Lecarme, Fannie Alloin

► To cite this version:

Sajad Rahimi, Lorenzo Stievano, Laetitia Dubau, Cristina Iojoiu, Lauréline Lecarme, et al.. Single-Atomic Dispersion of Fe and Co Supported on Reduced Graphene Oxide for High-Performance Lithium–Sulfur Batteries. ACS Applied Materials & Interfaces, 2023, 15 (38), pp.44932-44941. 10.1021/acsami.3c08669 . hal-04227549

HAL Id: hal-04227549

<https://hal.science/hal-04227549>

Submitted on 3 Oct 2023

HAL is a multi-disciplinary open access archive for the deposit and dissemination of scientific research documents, whether they are published or not. The documents may come from teaching and research institutions in France or abroad, or from public or private research centers.

L'archive ouverte pluridisciplinaire **HAL**, est destinée au dépôt et à la diffusion de documents scientifiques de niveau recherche, publiés ou non, émanant des établissements d'enseignement et de recherche français ou étrangers, des laboratoires publics ou privés.

Single atomic dispersion of Fe and Co supported on reduced graphene oxide for high performance lithium sulfur battery

Sajad Rahimi^a, Lorenzo Stievano^{b,c}, Laetitia Dubau^a, Cristina Iojoiu^{a,c}, Lauréline Lecarme^a, Fannie Alloin^{a,c*}

^a Univ. Grenoble Alpes, Univ. Savoie Mont Blanc, CNRS, Grenoble INP, LEPMI, 38000 Grenoble, France

^b ICGM, Univ. Montpellier, CNRS, ENSCM, 1919 route de Mende, 34293 Montpellier, France

^c Réseau sur le Stockage Electrochimique de l'Energie (RS2E), CNRS, FR3459, 80 039 Amiens Cedex, France

ABSTRACT:

High theoretical energy density and low cost make lithium-sulfur (LSB) batteries a promising system for next-generation energy storage. LSB performance largely depends on efficient reversible conversion of elemental sulfur to Li_2S . Here, well-designed sulfur host materials including Fe or Co single atoms embedded on N-doped reduced graphene oxide (MNC/G with $M = \text{Fe}, \text{Co}$) are proposed to tackle the LSB challenges and enhance its electrochemical performance. Using a combination of, Mössbauer spectroscopy and high-resolution scanning electron microscopy (HR-STEM), the atomic dispersion of Co and Fe was revealed up to relatively high mass loadings. After optimization of the electrolyte/sulfur (E/S) ratio, FeNC/G shows the most promising cycle performance combining a constant high discharge capacity at low E/S values with the lowest polarization. In particular, the material FeNC/G@S with a

high sulfur loading (9.4 mg cm^{-2}) delivers a high area capacity of 7.7 mAh cm^{-2} under lean electrolyte condition (6 mL g^{-1}).

KEYWORDS: Lithium sulfur battery, Sulfur host materials, FeNC catalyst, CoNC catalyst, lean electrolyte

1. INTRODUCTION

Owing to their high energy density, high theoretical capacity, low-cost and the nontoxicity of elemental sulfur, lithium-sulfur batteries (LSB) have been considered as a promising alternative to lithium-ion systems^{1,2}. For their practical application, however, some challenges such as: i) the poor electronic conductivity of sulfur and of its discharge products, ii) the volume expansion/contraction occurring during cycling, iii) the migration of soluble lithium polysulfide species (LiPS) in the electrolyte, also known as “LiPS shuttle effect”, and iv) the instability of the lithium/electrolyte interface, have to be overcome³.

Focusing on the cathode side, many efforts have been made to enhance the sulfur utilization and improve the cyclability of LSB. Physical confinement of sulfur in highly porous carbonaceous materials with different types of porous topologies such as graphene⁴, carbon^{5,6}, carbon nanotubes⁷ or/and chemisorption by employing heteroatoms-doped carbon backbones^{8,9} such as nitrogen¹⁰, sulfur^{11,9}, oxygen¹² were proposed to improve the reactivity of sulfur and mitigate LiPS diffusion in the electrolyte. In spite of these efforts, the results are still unsatisfactory: in fact, focusing only on heteroatoms-doping without considering the sluggish reaction kinetics would not fully address the above-mentioned challenges¹³. Moreover, to obtain LSB with a high energy density, it is necessary to minimize the electrolyte/sulfur (E/S) ratio while maximizing the sulfur content^{14,15}, which leads to even poorer reaction kinetics and uncompleted Li_2S_2 to Li_2S conversion.

The introduction of more efficient optimized carbon hosts for sulfur is therefore necessary to enhance the LSB performance under lean electrolyte conditions and high sulfur loadings. In recent works, the effect of various catalytic species, introduced to promote the conversion of LiPS species¹⁶⁻²⁰ while blocking their shuttling, have been investigated. However, while different compounds such as cobalt nanoparticles^{21,22}, metal oxides²³⁻²⁵ and sulfides^{26,27} have been proposed, the observed performance is still too low for a practical application.

Recently, single-atom catalysts based on earth-abundant transition metals (*e.g.*, Co, Fe, V, Cu) supported on nitrogen-doped carbon materials have been investigated as an auspicious alternative to noble metals catalysts for CO₂ reduction²⁸, Oxygen Reduction Reaction (ORR)²⁹⁻³¹, hydrogen evolution³² and more recently to increase the oxidation and reduction kinetics of sulfur and polysulfides compounds in Li-S battery^{1,33-36}. This class of materials could be, in principle, also a promising sulfur host material for LSB given their high electrical conductivity, catalytic activity, and their strong chemisorption ability toward LiPS originating from excellent π - π conjugated electron transfer inside the carbon network³⁷.

Herein, Fe and Co single atoms dispersed in N-containing carbon structures supported on a reduced graphene oxide scaffold (FeNC/G, CoNC/G) are proposed as sulfur host materials for LSB. One of the aims of this work was to increase the number of single atoms as much as possible in order to obtain catalytic properties vs PSs conversion/formation, already demonstrated^{1,35}, in a lean electrolyte. Indeed, the use of lean electrolyte condition is essential for achieving high energy density in Li-S batteries. A second objective was to compare two promising single atoms as catalyst, Fe and Co, using the same synthesis strategy. Several reasons can be brought to support the promising properties of such systems: 1) the simultaneous carbon doping with N and M to improve LiPS chemisorption using the 2,4,6-tri(2-pyridyl)-1,3,5-triazine (TPTZ) as soluble ligand. 2) the use of reduced graphene oxide as the carbon support, providing mechanical stability and high electrical conductivity, 3) the

introduction of catalytic species to promote the sluggish kinetics of LiPS conversion, 4) the use of an environmentally friendly route to obtain a single-atom dispersion of Fe and Co at the large scale and 5) the preparation of a carbon scaffold with high BET surface area, interconnected channels to enhance Li^+ diffusion and homogeneous distribution of the metals inside a 3D structure using NaCl as an inert template. Indeed, owing to its cubic structure, the NaCl template leads to the formation of compact carbon structure, which can thus be transferred to the final material with a high efficiency during the controlled decomposition of M-TPTZ/G during pyrolysis at 900°C ³⁸. In addition, the NaCl template can be easily eliminated, and permits the preparation of the M-TPTZ/G precursor with a good yield.

In this paper, we investigated the roles of Fe and Co single atoms on LiPS conversion under severe conditions (high sulfur loading and lean electrolyte). High Resolution High-angle annular dark-field (HR-HAADF) imaging in an aberration-corrected scanning electron microscopy (STEM) and Mössbauer spectroscopy were employed to identify the morphology, valence state, and coordination configuration of Fe and Co single atoms at the atomic level. The catalytic behavior of CoNC/G and FeNC/G toward LiPS conversion was evaluated by electrochemical study. The calculated rate constant k^0 shows that CoNC/G, compared to FeNC/G, effectively boosts the kinetic of LiPSs conversion leading to higher efficiency in converting S_8 to Li_2S_6 . After sulfur impregnation, the electrochemical performance of FeNC/G@S and CoNC/G@S composites was evaluated under severe conditions of S mass loading and lean electrolyte condition.

2. Materials and methods

2.1. FeNC/G, CoNC/G synthesis. 100 mg of 2,4,6-tri(2-pyridyl)-1,3,5-triazine (TPTZ) (Acros 99%) were dissolved in 25 mL of HCl (Fisher chemical ~37%) then 21.8 mg of Co (NO_3)₂6H₂O (Merck) or 13 mg of Fe(ac)₂ (Acros, 95%) (to have the 1/3 molar ratio of M to TPTZ) were added to synthesize CoNC/G and FeNC/G respectively. After 5 hours to allow

the thorough chelation of the metal ions by TPTZ, 12.5 mL of Graphene Oxide (GO) (6 mg mL⁻¹) were added. The suspension was stirred overnight, then 40 wt% of NaCl (Fisher Chemical 99%) were added. The solutions were immediately frozen by liquid N₂ and freeze-dried at -50°C to remove the solvents.

The pyrolysis step was performed in a tube furnace at 900 °C with a heating rate of 10 °C/min under a N₂ gas flow of 50 cm³ min⁻¹. After cooling down to room temperature, the recovered black powder was leached first with distilled water to remove the NaCl and then with 0.5 or 1 M HCl solution at 25 °C to remove metal and metal oxide particles. The acidic suspensions were washed with distilled water until reaching a neutral pH. The resulting powders FeNC/G, CoNC/G were dried at 60 °C overnight. For comparison, FeNC and CoNC materials, N-doped rGO, (NC/G), were synthesized without graphene oxide or metal precursor, respectively with the same procedure.

2.2. FeNC/G, CoNC/G@S preparation. FeNC/G and CoNC/G were impregnated with sulfur (ratio 2/3) (Alfa Aesar A7558) using the melt-diffusion strategy (2 h at 160 °C) to obtain the FeNC/G@S and CoNC/G@S composites with the sulfur content of 64 wt% determined by thermogravimetric analysis.

2.3 Material Characterization. X-Ray Powder Diffraction (XRD) was carried out on PANalytical X'Pert PRO MPD diffractometer with Cu K α radiation ($\lambda = 1.54178$ Å). The morphology of the materials was characterized by scanning electron microscopy (SEM KARL ZEISS Ultra 55). Conventional transmission electron microscopy (TEM) images were obtained by using a JEOL 2010 TEM microscope operated at 200 kV with a resolution of 0.19 nm. Atomically dispersed Fe and Co were observed with a Nion UltraSTEM 200 microscope equipped with an C₃/C₅ aberration corrector operated at 60 kV. ⁵⁷Fe Mössbauer spectra were measured using a conventional constant acceleration spectrometer and a commercial 2GBq ⁵⁷Co:Rh γ -ray source. Both the sample and the absorber were kept at room temperature in

ambient atmosphere. The velocity calibration was performed using an α -iron absorber, and the isomer shift (δ) values are given relative to α -Fe metal. X-ray photoelectron spectroscopy (XPS) measurement were conducted on Thermo Scientific K-Alpha. The Brunauer-Emmett-Teller (BET) surface area was obtained by using an ASAP 2020 Plus 2.0.

2.4. Electrochemical Measurements

2.4.1. Preparation of Lithium Polysulfides (Li_2S_6)

Lithium metal, and sulfur (S_8) were added in a stoichiometric volume ratio to a solvent mixture of 1,3-dioxolane (DOL, anhydrous, 99.8%, Aldrich) and 1,2-dimethoxyethane (DME, Alfa Aesar). The solution was stirred for 48 h to yield a solution of 0.1 M Li_2S_6 .

2.4.2. Catalytic effect evaluation- Cyclic voltammetry

In order to demonstrate the advantage of the FeNC/G and CoNC/G catalyst on the kinetic of LiPS conversion processes, Cyclic Voltammetry (CV) in a three-electrodes configuration was carried out on a BiologicVMP300 at different scan rates (10 to 70 mV.s^{-1}) between 2.8 and $2 \text{ V vs. Li}^+/\text{Li}$. The working electrode was obtained by mixing FeNC/G or CoNC/G materials and poly(vinylidene fluoride) (PVDF, Solvay Solef 6020/1001), in a ratio $8/2$. Several drops of N-methyl-2-pyrrolidone (NMP, AcroSeal) were added to obtain a homogeneous ink casted on platinum electrode (2 mm in diameter with $0.3\text{-}0.4 \text{ mg}$ of active materials). A protected Li metal electrode was used as the reference and counter electrodes and 10 mM of Li_2S_6 in DME: DOL ($1:1$) was used as the electrolyte.

2.4.3. Cell Assembly and Electrochemical Measurements

Electrodes were prepared by the following formulation: $80 \text{ wt.}\%$ of sulfur composite, $10 \text{ wt.}\%$ of SuperP (TIMCAL Super C65), and $10 \text{ wt.}\%$ of PVDF in NMP. The ink was tape casted on a carbon coated Al current collector and dried at 40°C overnight. CR2032 coin cells were used to evaluate the electrochemical performance vs. Li metal electrode. Celgard® 2335

impregnated with 1.0 M LiTFSI and 0.2 M LiNO₃ in DOL: DME (1:1 in vol.) electrolyte is used as electrolyte.

3. Results and discussion

3.1 MNC/G (M: Fe, Co) sulfur host materials

The design of a porous carbon with a high surface area allows the preparation of MNC materials with high metal loadings without the formation of agglomerated metal species, thus a high concentration of catalytic active sites for LiPS conversion was targeted.

CoNC/G, with a Co content of 8.4 wt%, determined by Atomic Absorption Spectroscopy (AAS), was obtained from a precursor solution containing a Co/TPTZ ratio of 1/3. As shown in **Figure S1**, part of the Co forms separate particles, which were eliminated by leaching the composite with HCl aqueous solutions. After leaching, the Co loading decreases to 6.2 wt% and 4.8 wt% using 0.5 M and 1 M HCl solutions, respectively. Only washing with 1 M HCl efficiently eliminates these cobalt particles (**Figure S1**). The Co loading is a high value in comparison with previous reports^{1,39} but the amount obtained is lower than the one obtained by Li et al.⁴⁰ which used a salt-template method. However, this reasonable mass percentage will make it possible to compare with Fe single atom catalysts, which are more difficult to obtain in high concentrations due to easy Fe atoms aggregation.

A similar approach was employed also for synthesis of FeNC/G. However, the preparation of composites with high Fe loadings remains a real challenge, since Fe atoms tend to aggregate during the pyrolysis step to form very stable species resistant to acid leaching such as Fe₃C, Fe₃N or Fe(CN)₆. Therefore, to obtain an atomic dispersion of the Fe with high Fe loadings, it is necessary to further optimize the Fe/TPTZ ratio, knowing that TPTZ is able to strongly chelate the Fe atoms and limit their motion during pyrolysis. XRD patterns of FeNC/G (**Figure S2**) show that when a Fe/TPTZ ratio of 1/3 is used for the synthesis, even with 1M HCl solution acid leaching, crystalline phase still exists. Only by using a Fe/TPTZ ratio of

1/4, it was possible to obtain completely amorphous carbon (**Figure S2**). The iron loading, determined by AAS analysis, is around 3 wt%, a remarkably high value in comparison with previous reports^{41,42} which proves the high efficiency of the synthesis protocol.

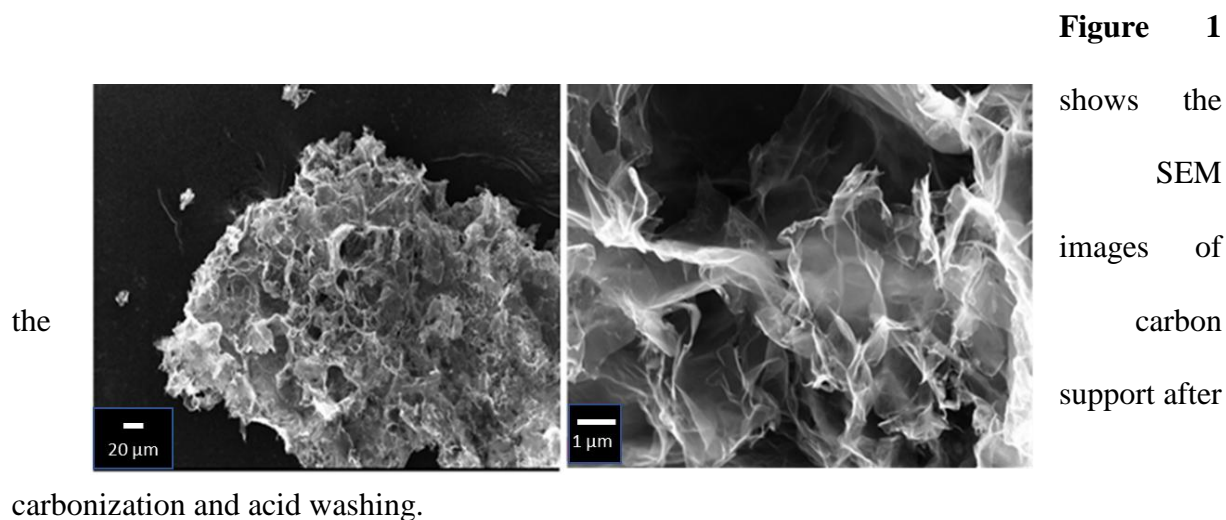
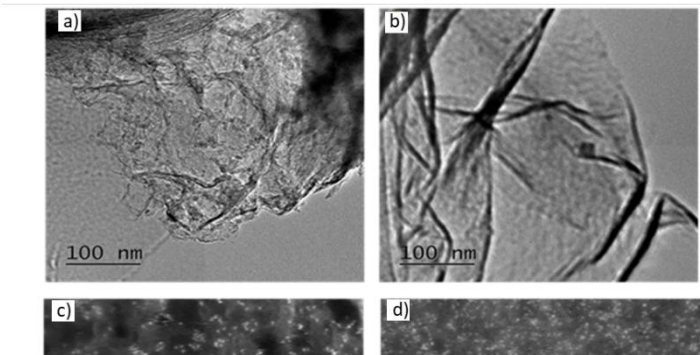


Figure 1: SEM Images of FeNC/G after carbonization and acid washing.

The observed 3D cage-like carbon morphology obtained at this stage clearly testifies the efficiency of the use of the NaCl cubic template. This morphology provides a high surface area for sulfur encapsulation by maximizing the contact between sulfur and catalyst enriched carbon.

The TEM images, of the FeNC/G (**Figure 2a**) and



CoNC/G catalysts (**Figure 2b**) clearly show the rGO sheets without presence of any M-derived nanoparticles, crystals or any clusters.

Figure 2: TEM images of a) FeNC/G, and b) CoNC/G. HR-STEM-HAADF images of c) FeNC/G and d) CoNC/G.

Atomically resolved HR-HAADF STEM was carried out on the two samples (**Figure 2c, d**) to reveal the metal dispersion in CoNC/G, FeNC/G at the atomic scale, as the image contrast is sensitive to the atomic number Z . The HAADF-STEM results clearly confirm the presence of atomically dispersed Fe and Co, identified as homogeneously distributed bright spots in the carbon structure for both Co- and Fe-based compounds. The density of Co atoms is higher than that of the Fe ones, in accordance with the higher Co loading.

The room-temperature ^{57}Fe Mössbauer spectrum of FeNC/G (**Figure 3**) reveals the presence of at least two quadrupole doublets, and is very similar to those usually observed for iron-based catalysts for oxygen electro-reduction reaction^{43,44}. As in these studies, the two quadrupole doublets, usually labelled as D1 ($QS = 0.93 \text{ mm s}^{-1}$, $IS = 0.35 \text{ mm s}^{-1}$) and D2 ($QS = 2.54 \text{ mm s}^{-1}$, $IS = 0.68 \text{ mm s}^{-1}$), have relative resonance areas of 60 and 40 %, and can be assigned to isolated oxidized $\text{Fe}^{\text{III}}\text{N}_4$, and to reduced low-spin and/or intermediate-spin square-planar $\text{Fe}^{\text{II}}\text{N}_4$ respectively²⁸. These results are coherent with the XRD and HAADF-

STEM results, confirming the atomic dispersion of the Fe and the absence of crystalline Fe species.

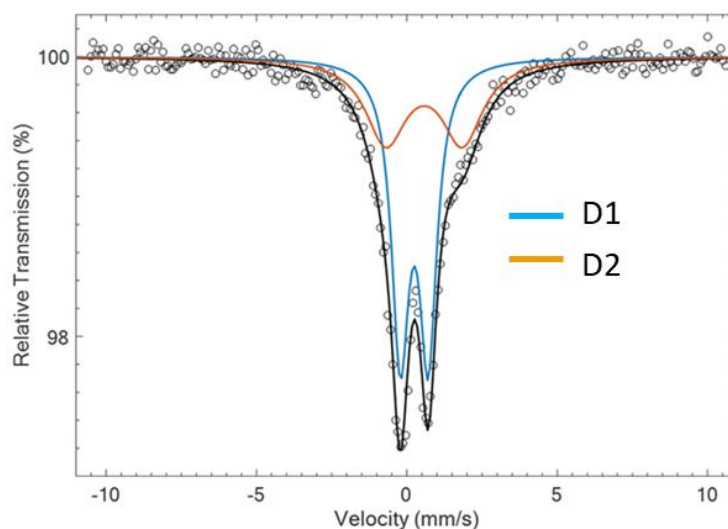


Figure 3: Mössbauer spectroscopy of FeNC/G structures. The circles and the black lines are the experimental and fitted data respectively.

The Fe or Co K-edge X-ray absorption near-edge structure (XANES) spectra of FeNC/G, CoNC/G and metal foil (Fe or Co) samples indicate the cationic states of Fe and Co centers in the composite. The XANES profile of CoNC/G with a pre-edge feature A at 7713 eV and a near-edge absorption energy (feature B at 7728 eV) (Figure S3) is in good accordance with the one reported for Co single atom catalysts¹. Regarding, the FeNC/G spectra, the profile (feature C at 7115 eV and D at 7133 eV) is also in good accordance with previous FeN₄ moiety on graphene based support⁴⁵ and in accordance with the Mössbauer spectroscopy.

The surface composition of CoNC/G and FeNC/G was investigated by XPS (**Figures S4 & S5**). The survey spectra (**Figures S4 & S5a**) show the presence of C, N and O in the two samples and the presence of Fe or Co in the Fe or Co-containing samples, respectively. The high resolution C1s spectra of CoNC/G and FeNC/G can be deconvoluted in several contributions with binding energies of 284.7±0.2, 285.3±0.2, 287.1±0.2, 288.6±0.2 and 290.8±0.2 eV, which can be assigned to sp² and sp³ carbon, C-N, O-C=O and π-π* satellites, respectively (**Figures S4 & S5b**). The N content of both FeNC/G and CoNC/G is around 10

wt.% at the surface of the material (**Figures S4 & S5a**). Such a high nitrogen content is expected to increase the polarity of the carbon, thus enhancing LiPS adsorption and mitigating their diffusion in the electrolyte. The high resolution N1s signal for CoNC/G and FeNC/G (**Figures S4 & S5c**) can be deconvoluted into six characteristic peaks at binding energies of 398.3 ± 0.2 , 399.1 ± 0.2 , 400.1 ± 0.2 , 400.9 ± 0.2 , 402.2 ± 0.2 , and 405.1 ± 0.4 eV, which correspond to, based on literature data, to pyridinic-N, metal-N, pyrrolic-N, graphitic-N, N-O, and NO_x , respectively^{29,38,46}, confirming the successful doping of carbon by nitrogen atoms. Consistent with the higher amount of Co atoms, the relative area of the metal-N peak is higher for CoNC/G than for FeNC/G, with 11.5% and 7.5% of the N1s signal respectively. The O1s signal for CoNC/G and FeNC/G (**Figures S3 & S4d**) can be deconvoluted into 3 characteristic peaks at binding energies of 531.3 ± 0.2 , 532.7 ± 0.2 and 535.4 ± 0.2 eV which correspond to, based on literature data, to C-O, C=O and absorbed oxygen in good accordance with the C1s spectra.

The $\text{Co}2p_{3/2}$ spectrum of CoNC/G, shown in **Figure S4e**, can be fitted by three components with binding energies 779.5 ± 0.3 , 781.9 ± 0.3 assigned to Co-C, Co-N respectively and a large signal at 785.8 ± 0.3 associated to the two $\text{Co}2p_{3/2}$ satellite compounds^{47,48}. The Fe2p spectrum (**Figure S5e**) can also be deconvoluted into three peaks for the $2p_{3/2}$ signal of Fe(II) and Fe(III) species at 709.1 ± 0.3 , 711.1 ± 0.3 eV and a broad peak at 714 ± 0.3 eV associated to the two Fe $2p_{3/2}$ satellite compounds. The Fe $2p_{1/2}$ ones are visible at 722.7 ± 0.3 and 725.4 ± 0.3 eV^{31,49}. The noisy signal did not allow to extract the contribution of the satellites. No peak at 708 eV was observed, which indicates the absence of a zero-valent Fe, which could be associate to iron carbides, at the surface of the sample.

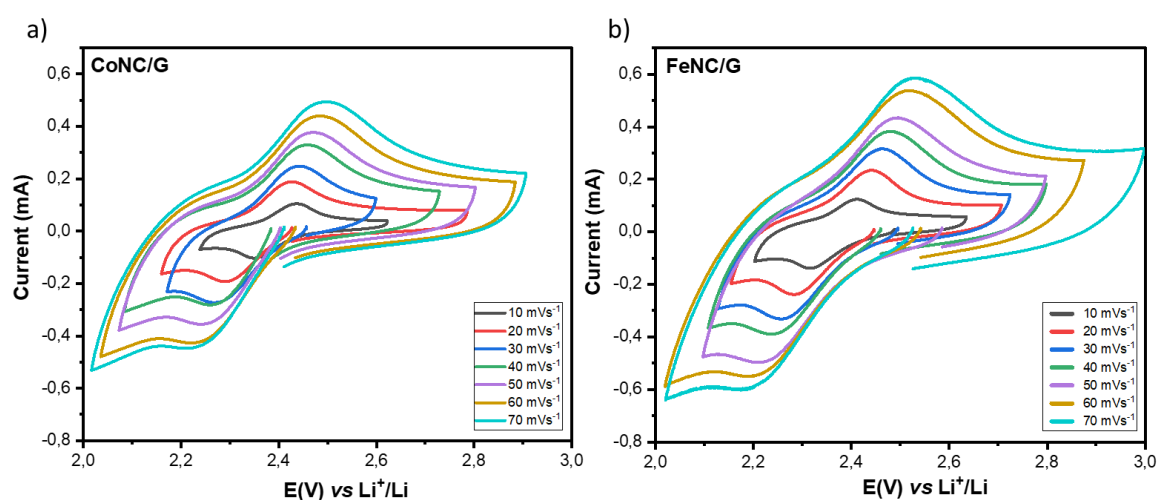
The Raman spectra of CoNC/G and FeNC/G, shown in **Figure S6**, reveal the characteristic D and G bands of carbon at around 1350 and 1590 cm^{-1} , respectively. The D band corresponds to defects in the graphitic structure of carbon while the G is ascribed to ordered-graphitic

structure. The intensity ratios of the D band and G band (I_D/I_G), equal to 1.22, and 1.48, respectively, confirm the highly defective/disordered nature of the carbon in the two composites. This characteristic can be also related to the high nitrogen-doping level of the carbon, with the nitrogen-rich sites binding to the metal species^{30,45}.

The BET surface areas (S_{BET}) of FeNC/G and CoNC/G were measured by N_2 physisorption for samples prepared from precursors containing different NaCl amounts. The N_2 adsorption-desorption isotherms of samples prepared from precursors containing 10 wt% of NaCl, shown in **Figure S7a**, exhibit a type I shape, include mainly micropores with pore sizes lower than 2 nm (**Figure S7c**). The total surface areas (S_A) of CoNC/G and FeNC/G, 68 and 86 $\text{m}^2 \text{g}^{-1}$, respectively. The two values are very similar, as the contribution of the metal species to the surface area is low. Increasing the NaCl content to 40 wt%, leads to an increase of the S_A to 334 $\text{m}^2 \text{g}^{-1}$ (**Figure S7b**), proving the positive templating effect of NaCl on the surface area without changing isotherm type (Type I) and pore size, mainly coming from rGO microporosities with pore sizes of about 2 nm. The host materials with the surface area of 334 $\text{m}^2 \text{g}^{-1}$ were used for the evaluation of the electrochemical performance. Such a high surface area, including bi-modal pore distribution, microporosity and macroporosity (pore size higher than 50 nm), should enhance the performance of LSB system by allowing sufficient space for the precipitation of Li_2S_2 and Li_2S in the sulfur electrode during the discharge, while physically entrapping the intermediate LiPS.

3.2 Catalytic Conversion of Li_2S_6 solution on FeNC/G, CoNC/G

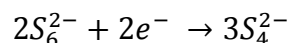
The kinetics of the LiPS conversion on FeNC/G and CoNC/G was studied by CV in three-electrodes configuration in the presence of a low concentration of soluble LiPS (10 mM of Li_2S_6 in DME: DOL, 1:1 in vol.). To extract information on the effect of the single atom catalysts on the kinetics of the process, the system was studied as a function of the scan rate. At low scan rate, a reversible electrochemical reaction can be observed with reduction peaks at 2.35 and 2.32 V vs Li^+/Li and the corresponding oxidation peaks at 2.43 and 2.40 V vs



Li^+/Li for CoNC/G and FeNC/G, respectively, thus with $\Delta E = 80$ mV (**Figure 4a & b**).

Figure 4: Cyclic voltammograms of a) CoNC/G and b) FeNC/G in 10 mM of Li_2S_6 at different scan rate.

Based on the combination of the electrochemical potential of the redox process and the number of electrons involved into the redox reaction, the electrochemical reduction process could be assigned to the reduction of S_6^{2-} to S_4^{2-} according to the reaction⁵⁰



The kinetic constants k° for the above reversible redox process calculated from the evolution of ΔE_{peak} at increasing scan rates using the Nicholson equation⁵¹ are 9.3×10^{-4} and $2.7 \times 10^{-4} \text{ cm s}^{-1}$ for CoNC/G, and FeNC/G, respectively. For comparison, the average k° value is $5 \times 10^{-3} \text{ cm s}^{-1}$ for a reversible process with high electron transfer kinetic such as the

ferrocinium/ferrocene couple⁵², *i.e.*, only about five time faster than polysulfide conversion on CoNC/G, showing that this material significantly enhances the kinetics of the conversion of long-chain polysulfides. In the case of FeNC/G, the value is slightly lower, but still promising, considering that the Fe loading in FeNC/G is more than 30 % lower than that of Co, in CoNC/G.

3.3 Electrochemical performance of the CoNC/G@S and FeNC/G@S composites

The behavior of the as-prepared CoNC/G and FeNC/G as host materials, for sulfur positive electrode was investigated in standard 2032 coin-cells containing CoNC/G@S and FeNC/G@S electrodes, lithium foil as the negative electrode and 1M LiTFSI and 0.2 M LiNO₃ in DOL:DME 1:1 in vol% as the electrolyte. The CV plots of the FeNC/G@S, and CoNC/G@S electrodes at 0.1 mV s⁻¹ (**Figure 5**) show a reversible behavior with two distinguished cathodic peaks at 2.25 and 1.90 V *vs.* Li⁺/Li associated to the conversion of elemental sulfur to long chain polysulfides (Li₂S_x, 8 ≤ x ≤ 4) and further reduction of long polysulfide chains to solid Li₂S₂ and Li₂S, respectively. In the subsequent anodic scan, two peaks appear at 2.40 and 2.60 V *vs.* Li⁺/Li attributed to the oxidation of short chains to long chain polysulfides and ultimately reformation of S₈. A slightly lower overpotential was observed for FeNC/G in the second region of LiPS conversion (LiPS to Li₂S₂/Li₂S) at this scan rate. The CV performed at higher scan rates (0.2 - 0.5 mV s⁻¹) for the CoNC/G@S and FeNC/G@S electrodes (**Figure S8a & b**), reveals an excellent reversibility of redox process confirming the promising behavior of the two catalysts in enhancing the conversion kinetics.

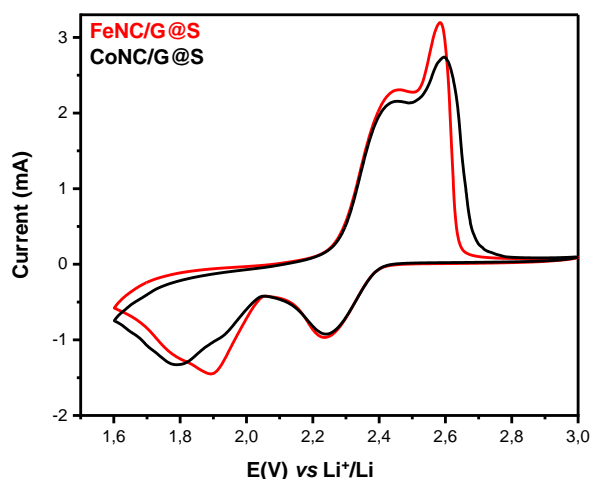


Figure 5: Cyclic voltammograms of CoNC/G@S, FeNC/G@S in 10 mM of Li_2S_6 at 0.1 mV s^{-1} .

At higher scan rate, the polarization obtained with the CoNC/G@S electrode is slightly lower than that observed with the FeNC/G@S electrode. In the conditions used for the CV studies, the two materials exhibit nearly the same electrochemical properties.

The first galvanostatic charge/discharge cycle at C/20 of the CoNC/G@S and FeNC/G@S electrodes at different E/S ratios is presented in **Figure 6a & b**. For CoNC/G@S, even at a low E/S ratio (6 mL g^{-1}), a discharge capacity close to 1100 mAh g^{-1} , *i.e.*, $\sim 65 \%$ of the theoretical capacity, was obtained with a sulfur loading of 4.5 mg cm^{-2} . The very similar capacities achieved at 8 and 6 mL g^{-1} and the theoretical ratio of the two plateaus suggest that the amount of formed Li_2S is mainly limited by the accessibility of sulfur active material. The surface area of the host material seems to be sufficient for the deposition of Li_2S .

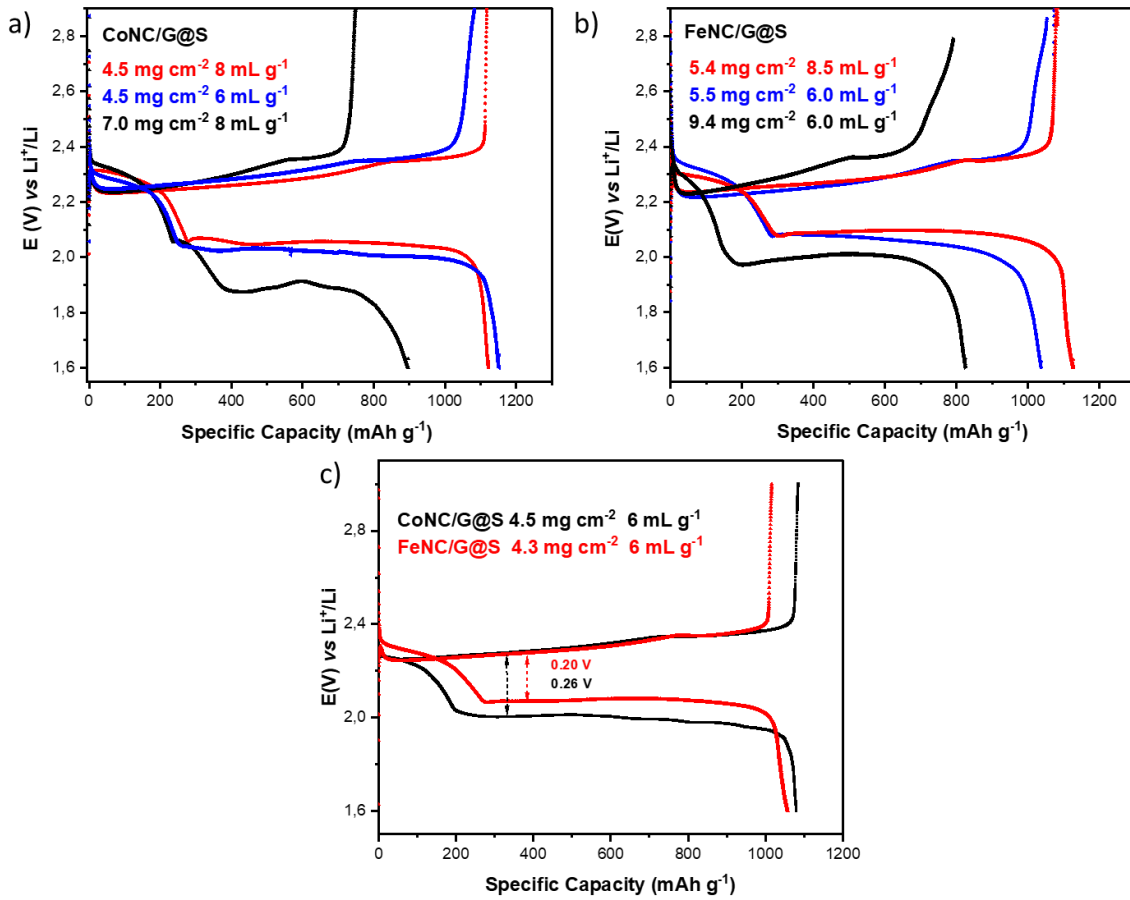


Figure 6: The GCPL curves for several sulfur loadings and E/S ratios of a) CoNC/G@S and b) FeNC/G@S at C/20. c) The GCPL curves of CoNC@S, FeNC @S at C/20, loading $\sim 4.4 \text{ mg cm}^{-2}$, E/S = 6 mL g^{-1} .

The reversible capacity decreases to 900 mAh g^{-1} at 6.3 mAh cm^{-2} upon increasing the sulfur loading (7 mg cm^{-2} , electrode thickness $85 \text{ }\mu\text{m}$, E/S = 6 mL g^{-1}), which confirms the promising performance of CoNC/G as a host material allowing a high sulfur utilization. It is worth mentioning that the discharge curve for high loading manifest several plateaus and polarization, indicating a further differentiation of the electrochemical reaction potentials in high viscous electrolyte due to kinetic limitation.

Similar results were obtained also for FeNC/G@S (**Figure 6b**) for which the promising capacity of 1110 mAh g^{-1} (66% of the theoretical capacity) is obtained with a S loading of $\sim 5.5 \text{ mg cm}^{-2}$ at E/S ratios of 8.5 and 6 mL g^{-1} , confirming that FeNC/G enhances the utilization of sulfur under lean electrolyte conditions.

Similar charge curves are observed for the two E/S ratios, even though the plateau associated with the oxidation of the long chain LiPSs is longer for E/S = 8.5 mL g⁻¹ compared to E/S = 6 mL g⁻¹ (~850 mAh g⁻¹ vs. ~750 mAh g⁻¹), due to the shuttle effect which is more favorable in less viscous medium. By increasing the electrode thickness of the FeNC/G@S to 9.4 mg cm⁻² (thickness 95-100 μm), only slightly more polarized discharge curves are obtained with a ratio E/S = 6 mL g⁻¹ and a current density of 7.7 mAh cm⁻². Under these conditions, the high capacity of 824 mAh g⁻¹ (50% of the theoretical capacity) is obtained. These results confirm the very good performance of FeNC/G as a sulfur host also for thick electrode, providing a high sulfur utilization under lean electrolyte condition. High overpotential and low sulfur utilization at high S mass loadings (thick electrodes) has already been reported. In fact, these behaviors may have several explanations such as (i) the sluggish kinetic of the sulfur reduction under lean electrolyte condition⁵³, which can be attributed to the low solubility of LiPSs and the mass transport limitation of both polysulfide anions and Li⁺ cations in concentrated viscous electrolytes, more detrimental for thick electrodes, (ii) the less efficient electron percolation in thick electrodes and (iii) the ohmic drop due to the high applied current. Nevertheless, reaching a sulfur utilization of 50% for a heavily loaded FeNC/G@S electrode proves the promising performance of the FeNC/G host materials.

The effect of the electrode thickness was pushed to its limits by testing a FeNC/G@S electrode with ultra-high sulfur loading (13 mg cm⁻²) under lean electrolyte condition (E/S = 4.9 mL g⁻¹). Under these conditions, a very high areal capacity of 9 mAh cm⁻² is obtained at C/50 (**Figure S9**), with a sulfur utilization of ~ 40 % (capacity of the first plateau), and a practical capacity of 692 mAh g⁻¹ (i.e. ~ 40% of the theoretical capacity). As expected, by increasing the S loading and decreasing the E/S ratio, the drawbacks observed previously are amplified. Moreover, given the very slow C-rate, the shuttle effect is significant but only for the first cycle. The passivation of the lithium interface and the properties of FeNC/G such as

chemisorption, in a small extent (**Figure S10**), and physical confinement (large amount of microporosity) mitigate the polysulfide diffusion and enable a reversible behavior at C/50 for the second cycle and at C/20 for the following cycles. At C/20, an increase of the polarization and a good coulombic efficiency (~ 0.98) are obtained with an areal capacity of 6 mAh cm^{-2} (460 mAh g^{-1}).

The effect of the nature of the transition metal on the polarization was tested by comparing FeNC/G@S and CoNC/G@S electrodes with the same S loading under the same lean electrolyte conditions. As shown in **Figure 6c**, FeNC/G provides lower polarization than CoNC/G (0.2 vs. 0.26 V, respectively). These results do not contradict the observed better performance of CoNC/G in the conversion of Li_2S_6 to Li_2S_4 in diluted solution, as LSB system includes several steps of conversion with kinetics mainly dependent of the electrolyte amount which impact its viscosity, the ratio of solid lithium sulfides, the composition in the different LiPS and the mass transport, in short the overall kinetic of the reaction.

Further investigations were carried out to better understand the influence of the different components of each host material compound on the electrochemical performance. For instance, the properties of the FeNC@S and CoNC@S electrodes prepared without rGO were tested in galvanostatic cycling (**Figure S11**). For electrodes with a sulfur loading of 3 mg cm^{-2} , the highest possible loading reached for such composite's electrode without cracks, a high E/S ratio must be used (8 and 10 mL g^{-1} for FeNC@S and CoNC@S respectively) in order to obtain a sulfur utilization of 60%. Moreover, a high polarization is observed, indicating a limited contact between the electrolyte and the sulfur active material under lean electrolyte condition, as well as a poor electronic conductivity. Indeed, the deposition of TPTZ metal complex on the rGO nanosheets forms a high electronic conductivity network, while the high microporosity of rGO enhances the electrolyte up-take and improves the sulfur utilization.

The positive effect of the metal centers on the LiPS conversion was verified by testing a metal-less NC/G@S electrode with a sulfur loading of 5.1 mg cm^{-2} and two E/S ratios (13 and 6 mL g^{-1}) (**Figure S12**). The electrode under lean electrolyte conditions exhibits poor performance, especially in the region associated to the conversion of LiPS to $\text{Li}_2\text{S}_2/\text{Li}_2\text{S}$ (second discharge plateau). The increase of the amount of electrolyte induces a decrease in polarization, which might also be due to the decrease in viscosity (increasing mass transport) and the increase of the solubility of LiPSs, with the consequence to improve the kinetics of their conversion. A discharge capacity of 1240 mAh g^{-1} is obtained at C/20 for a E/S ratio of 13 mL g^{-1} , with a higher polarization than with the metal-containing hosts, however. In addition, independently of the E/S ratio, the charge capacity is significantly lower than the discharge one, indicating a weak LiPSs retention ability of this electrode. In summary, the combination of rGO with a highly dispersed supported metal, independently of the nature of the latter, significantly improves the performance of the LSB under lean electrolyte conditions.

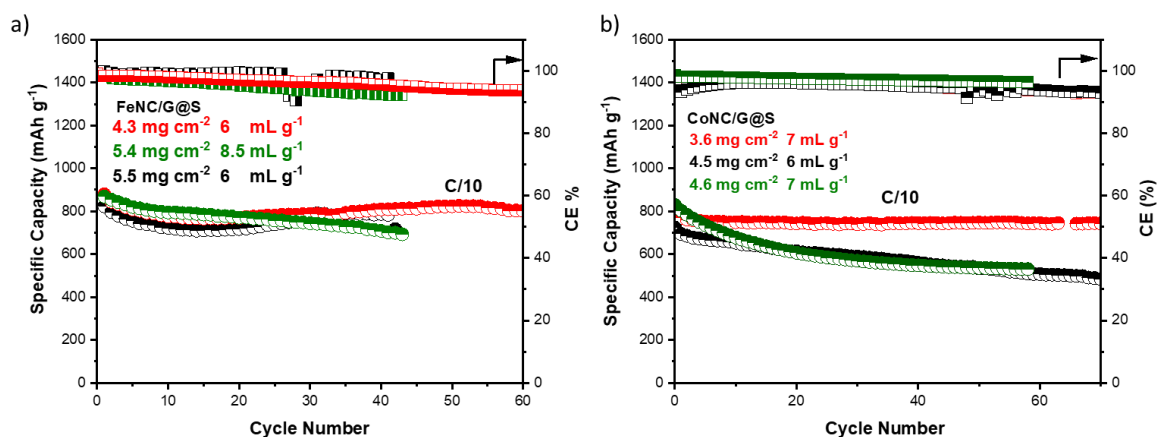


Figure 7: The long-term cycling of a) CoNC/G@S electrodes and b) FeNC/G@S electrodes, at C/10.

The long-term cycling performance of several FeNC/G@S and CoNC/G@S electrodes is shown in **Figure 7a & b**. All tested material, based on both CoNC/G and FeNC/G, manifest promising cycle stabilities. For example, the electrode based on CoNC/G@S (3.6 mg cm^{-2} ,

E/S = 7 mL g⁻¹) manifests promising cycle stability at C/10 over more than 70 cycles (~81% capacity retention).

An increase of the S loading up to 4.5 mg cm⁻² in lean electrolyte E/S ≤ 6, however, induces a significant increase of the capacity fading (**Figure 7b**). For high loading, the electrodes based on FeNC/G seems to exhibit a higher cycle stability than the CoNC/G based electrode. Indeed, FeNC/G@S and CoNC/G@S electrodes with similar thickness and electrolyte amounts (~ 4.5 mg cm⁻² and 6 mL g⁻¹) exhibit capacity retentions of 93 % and 62 % of the initial capacity after 60 cycles, respectively (**Figure 7a & b**). The higher capacity retention of FeNC/G@S electrode compared to CoNC/G@S, in severe conditions, might be due to the more effective interaction of PS anions with FeNC/G than with CoNC/G, which has an effect on both LiPS retention ability and reaction kinetics. Indeed, the calculated binding energies between Li₂S₆ and FeN₂ (E_{ads} = -1.794 eV) or FeN₄, (E_{ads} = -1.352 eV)⁵⁴ are sensibly higher than those between CoNC and Li₂S₆ (E_{ads} = - 0.50 eV)⁴⁵. The E/S ratio has also a strong effect on the cycling performance. Indeed, the FeNC@S electrode with the S mass loading of ~ 5.5 mg cm⁻² and E/S ratio of 6 mL g⁻¹ shows better retention compared to the same electrode with a E/S ratio of 8 mL g⁻¹ (95 % compared to 79 % over 40 cycles) with higher coulombic efficiency (97 % compare to 91 % over 40 cycles). This significant improvement can be explained by the formation of highly viscous LiPS solutions, limiting the mobility of the soluble species far from the electrode and thus increasing the capacity retention.

It is worth mentioning that, the obtained electrochemical performance under sever conditions e.g., high S mass loading and lean electrolyte condition, by the CoNC/G, and FeNC/G host materials are competitive among the recent reports on lithium sulfur battery (Table S1), which may be associated with the high concentration of SACs and the large specific surface area of the carbon structure. Regarding the performance obtained and in accordance with the ones reported in the literature, Fe Single Atom is more efficient than Co single atom in high S mass

loading and lean electrolyte condition (Table S1), whereas for sulfur loading, $\leq 4 \text{ mg cm}^{-2}$, Co and Fe based SACs show equivalent performance.

4. Conclusion

In this work, sulfur electrode hosts containing atomically dispersed Fe and Co species were synthesized by a simple one step pyrolysis method, using rGO as the carbon support. Several physicochemical analyses including atomically resolved microscopy, XANES, XPS and Mössbauer spectroscopy allowed a thorough characterization of the synthesized materials. After impregnation with sulfur, the performance of these materials as positive electrodes for lithium sulfur battery was evaluated by studying the effect of several parameters such as the E/S ratio and the sulfur mass loading.

The results of this study show that the combination of a high-performance sulfur host material (MNC/G) with sulfur species enhances the electronic conductivity of the sulfur electrode, maximizes the ionic mobility into the 3D-electrode and ultimately enhances the utilization of sulfur under lean electrolyte conditions, thus delivering a high discharge capacity. The obtained high cycle stability is explained by the formation of a highly viscous electrolyte rich in LiPS species in intimate contact with the electrode host. While CoNC/G and FeNC/G give similar performance with large electrolyte/sulfur ratio, the catalytic property of Fe single atom in lean electrolyte and high sulfur loading is clearly superior, underlining the importance of evaluating S host structures under conditions of sulfur loading and electrolyte amount that allow high energy density to be achieved. Indeed, in severe conditions, the catalytic properties become essential and must be optimized, as the reaction mainly occurs in solid state in a thick electrode.

Supporting information

XRD, XANES, XPS, Raman, BET and electrochemical data including CV curves and GCPL.

Author information

Corresponding Author

Fannie Alloin - Univ. Grenoble Alpes, Univ. Savoie Mont Blanc, CNRS, Grenoble INP, LEPMI, 38000 Grenoble, France. Réseau sur le Stockage Electrochimique de l'Energie (RS2E), CNRS, FR3459, 80 039 Amiens Cedex, France ; orcid.org/0000-0001-7882-1587

E-mail: Fannie.alloin@grenoble-inp.fr

Authors

Sajad Rahimi - Univ. Grenoble Alpes, Univ. Savoie Mont Blanc, CNRS, Grenoble INP, LEPMI, 38000 Grenoble

Lorenzo Stievano - ICGM, Univ. Montpellier, CNRS, ENSCM, 1919 route de Mende, 34293 Montpellier, France. Réseau sur le Stockage Electrochimique de l'Energie (RS2E), CNRS, FR3459, 80 039 Amiens Cedex, France ; orcid.org/0000-0001-8548-0231

Laetitia Dubau - Univ. Grenoble Alpes, Univ. Savoie Mont Blanc, CNRS, Grenoble INP, LEPMI, 38000 Grenoble, France ; orcid.org/0000-0001-9520-1435

Cristina Iojoiu - Univ. Grenoble Alpes, Univ. Savoie Mont Blanc, CNRS, Grenoble INP, LEPMI, 38000 Grenoble, France ; orcid.org/0000-0002-5823-8025

Lauréline Lecarme - Univ. Grenoble Alpes, Univ. Savoie Mont Blanc, CNRS, Grenoble INP, LEPMI, 38000 Grenoble, France ; orcid.org/0000-0001-9360-9197

Author Contributions

Sajad Rahimi, methodology, experimental operation, data analysis, and writing; Lorenzo Stievano, Mössbauer analysis, and writing; Laetitia Dubau, TEM and HAADF analysis; Cristina Iojoiu, discussion and supervision; Lauréline Lecarme, discussion and supervision

and Fannie Alloin, supervision of the project, funding acquisition, data analysis, and writing. All the authors have approved the final version of the manuscript.

ACKNOWLEDGEMENTS

The authors thank C. Reibel (PAC-ICGM, Univ. Montpellier), for the magnetic measurements, M. T. Sougrati for the measurement of the ^{57}Fe Mössbauer spectra and V. Martin for the XPS measurement. The authors thank the ESRF SNBL beamline, D. Stoian and K. Marshall. For the XANES measurements. The authors acknowledge financial support from the CNRS-CEA “METSA” French network (FR CNRS 3507) on the platform LPS-STEM. This work has the financial support for the PhD of M. Rahimi Sajad, of the Centre of Excellence of Multifunctional Architected Materials "CEMAM" n° AN-10-LABX-44-01 and the financial support for the ANR project. N° ANR-18-CE05-0022-01. For the purpose of open access, the author has applied a CC-BY public copyright licence to any Author Accepted Manuscript (AAM) version arising from this submission.

REFERENCES

- [1] Du, Z., Chen, X. Hu, W., Chuang, C., Xie, S., Hu, A., Yan, W., Kong, X., Wu, X., Ji, H., Wan, L.-J. Cobalt in Nitrogen-Doped Graphene as Single-Atom Catalyst for High-Sulfur Content Lithium–Sulfur Batteries. *J Am Chem Soc* **2019**, *141*, 3977–3985. doi.org/10.1021/jacs.8b12973
- [2] Yin, Y.-X., Xin, S., Guo, Y.-G, Wan, L.-J. Lithium–sulfur Batteries: Electrochemistry, Materials, and Prospects. *Angew Chem Int Ed* **2013**, *52*, 13186–13200. doi.org/10.1002/anie.201304762
- [3] Manthiram, A. Fu, Y., Su, Y.-S. Challenges and Prospects of Lithium–sulfur Batteries. *Acc Chem Res* **2013**, *46*, 1125–1134. doi.org/10.1021/ar300179v
- [4] Yeon, J. S., Yun, S. Park, J. M., Park, H. S. Surface-Modified Sulfur Nanorods Immobilized on Radially Assembled Open- Porous Graphene Microspheres for Lithium–Sulfur Batteries. *ACS Nano* **2019**, *13*, 5163–5171. doi.org/10.1021/acsnano.8b08822
- [5] Qin, X., Wu, J., Xu, Z.L., Chong, W. G., Huang, J.-Q., Liang, G., Li, B., Kang, F., Kim, J.-K. Electrospayed Multiscale Porous Carbon Microspheres as Sulfur Hosts for Long-Life Lithium-Sulfur Batteries. *Carbon* **2019**, *141*, 16–24. doi.org/10.1016/j.carbon.2018.09.048
- [6] Feng, S., Song, J., Zhu, C., Shi, Q., Liu, D. Li, J., Du, D., Zhang, Q., Lin, Y. Assembling Carbon Pores into Carbon Sheets: Rational Design of Three-Dimensional Carbon Networks for a Lithium–Sulfur Battery. *ACS Appl. Mater. Interfaces* **2019**, *11*, 5911–5918. doi.org/10.1021/acsami.8b17549
- [7] Zhang, Y.-Z., Zhang, Z., Liu, S., Li, G.-R., Gao, X.-P. Free-Standing Porous Carbon Nanofiber/Carbon Nanotube Film as Sulfur Immobilizer with High Areal Capacity for

- Lithium–Sulfur Battery. *ACS Appl. Mater. Interfaces* **2018**, *10*, 8749–8757. doi.org/10.1021/acsami.8b00190
- [8] Cheng, D., Wu., P., Wang, J., Tang, X., An, T., Zhou, H., Zhang, D., Fan, T., Synergetic Pore Structure Optimization and Nitrogen Doping of 3D Porous Graphene for High Performance Lithium Sulfur Battery. *Carbon* **2018**, *143*, 31058–31061. doi.org/10.1016/j.carbon.2018.11.032
- [9] Du, L., Cheng, X., Gao, F., Li, Y., Bu, Y., Zhang, Z. Wu, Q., Yang, L., Wang, X., Hu, Z. Electrocatalysis of S-Doped Carbon with Weak Polysulfide Adsorption Enhances Lithium–Sulfur Battery Performance. *Chem. Commun.* **2019**, *55* (45), 6365–6368. doi.org/10.1039/C9CC02134E.
- [10] Chen, M., Le, T., Zhou, Y., Kang, F., Yang, Y. Thiourea-Induced N/S Dual-Doped Hierarchical Porous Carbon Nanofibers for High-Performance Lithium-Ion Capacitors. *ACS Appl. Energy Mater.* **2020**, *3* (2), 1653–1664. https://doi.org/10.1021/acsaem.9b02157.
- [11] Chabu, J.M., Zeng, K. Chen, W., Mustapha, A., Li, Y., Liu, Y.-N. A Novel Graphene Oxide-Wrapped Sulfur Composites Cathode with Ultra-High Sulfur Content for Lithium–Sulfur Battery. *Appl. Surf. Sci.* **2019**, *493*, 233–540. doi.org/10.1016/j.apsusc.2019.07.061
- [12] Ji, L., Rao, M., Zheng, H., Zhang, L., Li, Y., Duan, W., Guo, J., Cairns, E. J., Zhang, Y. Graphene Oxide as a Sulfur Immobilizer in High Performance Lithium/Sulfur Cells. *J. Am. Chem. Soc.* **2011**, *133* (46), 18522–18525. https://doi.org/10.1021/ja206955k.
- [13] Yu, Z., Lv, W., Lin, Q., Huang, X., Yang, Y. A (110) Facet-Dominated Vanadium Dioxide Enabling Bidirectional Electrocatalysis for Lithium–Sulfur Batteries. *ACS Nano* **2021**, *15*, 16878–16886. DOI: 10.1021/acsnano.1c07647
- [14] Mikhaylik, Y.V., Akridge, J.R. Polysulfide Shuttle Study in the Li/S Battery System. *J. Electrochem. Soc.* **2004**, *151*, A1969. DOI 10.1149/1.1806394
- [15] Xu, R., Lu, J., Amine, K. Progress in Mechanistic Understanding and Characterization Techniques of Li-S Batteries. *Adv. Energy Mater.* **2015**, *5* (16), 1500408. doi.org/10.1002/aenm.201500408.
- [16] Wang, R., Yang, J., Chen, X., Zhao, Y., Zhao, W., Qian, G., Li, S., Xiao, Y., Chen, H., Ye, Y., Zhou, G., Pan, F. Highly Dispersed Cobalt Clusters in Nitrogen-Doped Porous Carbon Enable Multiple Effects for High-Performance Li–S Battery. *Adv. Energy Mater.* **2020**, *10* (9), 1903550. doi.org/10.1002/aenm.201903550.
- [17] Deng, D.-R., Xue, F., Jia, Y.-J., Ye, J.-C., Bai, C.-D., Zheng, M.-S., Dong, Q.-F. Co4N Nanosheet Assembled Mesoporous Sphere as a Matrix for Ultrahigh Sulfur Content Lithium–Sulfur Batteries. *ACS Nano* **2017**, *11* (6), 6031–6039. doi.org/10.1021/acsnano.7b01945.
- [18] Yuan, H., Peng, H.-J., Li, B.-Q., Xie, J., Kong, L., Zhao, M., Chen, X., Huang, J.-Q., Zhang, Q. Conductive and Catalytic Triple-Phase Interfaces Enabling Uniform Nucleation in High-Rate Lithium–Sulfur Batteries. *Adv. Energy Mater.* **2019**, *9* (1), 1802768. doi.org/10.1002/aenm.201802768.
- [19] Huang, S., Lim, Y. V., Zhang, X., Wang, Y., Zheng, Y., Kong, D., Ding, M., Yang, S. A., Yang, H. Y. Regulating the Polysulfide Redox Conversion by Iron Phosphide Nanocrystals for High-Rate and Ultrastable Lithium-Sulfur Battery. *Nano Energy* **2018**, *51*, 340–348. doi.org/10.1016/j.nanoen.2018.06.052.
- [20] Xi, K., He, D., Harris, C., Wang, Y., Lai, C., Li, H., Coxon, P. R., Ding, S., Wang, C., Kumar, R. V. Enhanced Sulfur Transformation by Multifunctional FeS₂/FeS/S Composites for High-Volumetric Capacity Cathodes in Lithium–Sulfur Batteries. *Adv. Sci.* **2019**, *6* (6), 1800815. doi.org/10.1002/advs.201800815.
- [21] Zhang, M., Yu, C., Zhou, C., Song, X., Han, X., Liu, X., Hao, C., Qiu, J. Cobalt-Embedded Nitrogen-Doped Hollow Carbon Nanorods for Synergistically Immobilizing the Discharge Products in Lithium-Sulfur Battery. *Energy Storage Mater.* **2016**, *5*, 223–229. doi.org/10.1016/j.ensm.2016.04.002

- [22] Li, Y.-J., Fan, J.-M., Zheng, M.-S., Dong, Q.-F. A Novel Synergistic Composite with Multi-Functional Effects for High-Performance Li–S Batteries. *Energy Environ. Sci.* **2016**, 9 (6), 1998–2004. doi.org/10.1039/C6EE00104A.
- [23] Wang, Z.-Y., Wang, L., Liu, S., Li, G.-R., Gao, X.-P. Conductive CoOOH as Carbon-Free Sulfur Immobilizer to Fabricate Sulfur-Based Composite for Lithium–Sulfur Battery. *Adv. Funct. Mater.* **2019**, 29 (23), 1901051. doi.org/10.1002/adfm.201901051.
- [24] Wang, L., Song, Y.-H., Zhang, B.-H., Liu, Y.-T., Wang, Z.-Y., Li, G.-R., Liu, S., Gao, X.-P. Spherical Metal Oxides with High Tap Density as Sulfur Host to Enhance Cathode Volumetric Capacity for Lithium–Sulfur Battery. *ACS Appl. Mater. Interfaces* **2020**, 12 (5), 5909–5919. doi.org/10.1021/acsami.9b20111.
- [25] Liang, X., Hart, C., Pang, Q., Garsuch, A., Weiss, T., Nazar, L. F. A Highly Efficient Polysulfide Mediator for Lithium–Sulfur Batteries. *Nat. Commun.* **2015**, 6 (1), 5682. doi.org/10.1038/ncomms6682.
- [26] Wang, N., Chen, B., Qin, K., Liu, E., Shi, C., He, C., Zhao, N. Rational Design of Co₉S₈/CoO Heterostructures with Well-Defined Interfaces for Lithium Sulfur Batteries: A Study of Synergistic Adsorption-Electrocatalysis Function. *Nano Energy* **2019**, 60, 332–339. doi.org/10.1016/j.nanoen.2019.03.060.
- [27] He, J., Chen, Y., Manthiram, A. Metal Sulfide-Decorated Carbon Sponge as a Highly Efficient Electrocatalyst and Absorbant for Polysulfide in High-Loading Li₂S Batteries. *Adv. Energy Mater.* **2019**, 9 (20), 1900584. doi.org/10.1002/aenm.201900584.
- [28] Huan, T.N., Ranjbar, N., Rousse, G., Sougrati, M. T., Zitolo, A., Mougél, V., Jaouen, F., Fontecave, M. Electrochemical Reduction of CO₂ Catalyzed by Fe-N- C Materials: A Structure–Selectivity Study. *ACS Catal.* **2017**, 1520–1525. doi.org/10.1021/acscatal.6b03353
- [29] Mazzucato, M., Daniel, G., Mehmood, A., Kosmala, T., Granozzi, G., Kucernak, A., Durante, C. Effects of the Induced Micro- and Meso-Porosity on the Single Site Density and Turn over Frequency of Fe-N-C Carbon Electrodes for the Oxygen Reduction Reaction. *Appl. Catal. B Environ.* **2021**, 291, 120068. doi.org/10.1016/j.apcatb.2021.120068.
- [30] Zhang, H., Hwang, S., Wang, M., Feng, Z., Karakalos, S., Luo, L., Qiao, Z., Xie, X., Wang, C., Su, D., Shao, Y., Wu, G. Single Atomic Iron Catalysts for Oxygen Reduction in Acidic Media: Particle Size Control and Thermal Activation. *J. Am. Chem. Soc.* **2017**, 139 (40), 14143–14149. doi.org/10.1021/jacs.7b06514.
- [31] Sun, M., Davenport, D., Liu, H., Qu, J., Elimelech, M., Li, J. Highly Efficient and Sustainable Non-Precious-Metal Fe–N–C Electrocatalysts for the Oxygen Reduction Reaction. *J. Mater. Chem. A* **2018**, 6 (6), 2527–2539. doi.org/10.1039/C7TA09187G.
- [32] Fei, H., Dong, J., Arellano-Jiménez, M. J., Ye, G., Dong Kim, N., Samuel, E. L. G., Peng, Z., Zhu, Z., Qin, F., Bao, J., Yacaman, M. J., Ajayan, P. M., Chen, D., Tour, J. M. Atomic Cobalt on Nitrogen-Doped Graphene for Hydrogen Generation. *Nat. Commun.* **2015**, 6 (1), 8668. doi.org/10.1038/ncomms9668.
- [33] Zhou, G., Zhao, S., Wang, T., Yang, S.-Z., Johannessen, B., Chen, H., Liu, C., Ye, Y., Wu, Y., Peng, Y., Liu, C., Jiang, S. P., Zhang, Q., Cui, Y. Theoretical Calculation Guided Design of Single-Atom Catalysts toward Fast Kinetic and Long-Life Li–S Batteries. *Nano Lett.* **2020**, 20, 1252–1261. doi.org/10.1021/acs.nanolett.9b04719
- [34] Xiao, R., Yu, T., Yang, S., Chen, K., Li, Z., Liu, Z., Hu, T., Hu, G., Li, J., Cheng H.-M., Sun, Z. Li, F. Electronic structure adjustment of lithium sulfide by a single-atom copper catalyst toward high-rate lithium-sulfur batteries. *Energy Storage Materials* **2022**, 51, 890–899. doi.org/10.1016/j.ensm.2022.07.024
- [35] Li, Y., Chen, G., Mou, J., Liu, Y., Xue, S., Tan, T., Zhong, W., Deng, Q., Li, T., Hu, J., Yang, C., Huang, K., Liu, M., Cobalt single atoms supported on N-doped carbon as an active and resilient sulfur host for lithium–sulfur batteries. *Energy Storage Materials* **2020**, 28, 196–204. doi.org/10.1016/j.ensm.2020.03.008

- [36] Wang, J., Han, W.-Q. A Review of Heteroatom Doped Materials for Advanced Lithium–Sulfur Batteries. *Adv. Funct. Mater.* **2022**, 32, 3107166. doi.org/10.1002/adfm.202107166
- [37] Jeong, B., Shin, D., Jeon, H., D. Ocon, J., Mun, B. S., Baik, J., Shin, H.-J., Lee, J. Excavated Fe-N-C Sites for Enhanced Electrocatalytic Activity in the Oxygen Reduction Reaction. *ChemSusChem* **2014**, 7, 1289–1294. doi.org/10.1002/cssc.201301374
- [38] Guo, C., Li, Y., Liao, W., Liu, Y., Li, Z., Sun, L., Chen, C., Zhang, J., Si, Y., Li, L. Boosting the Oxygen Reduction Activity of a Three-Dimensional Network Co–N–C Electrocatalyst *via* Space-Confined Control of Nitrogen-Doping Efficiency and the Molecular-Level Coordination Effect. *J. Mater. Chem. A* **2018**, 6 (27), 13050–13061. doi.org/10.1039/C8TA03759K.
- [39] Li, B.-Q. Kong, L., Zhao, C.-X., Jin, Q., Chen, X., Peng H.-J., Qin J.-L., Chen J.-X., Yuan, H., Zhang, Q., Huang J.-Q. Expediting redox kinetics of sulfur species by atomic-scale electrocatalysts in lithium–sulfur batteries, *InfoMat* **2019**, 1 (4), 522–541. doi.org/10.1002/inf2.12056
- [40] Li, Y., Wu, J., Zhang, B., Wang, W., Zhang, G., Seh, Z. W., Zhang, N., Sun, J., Huang, L., Jiang, J., Zhou, J., Sun, Y. Fast Conversion and Controlled Deposition of Lithium (Poly)Sulfides in Lithium-Sulfur Batteries Using High-Loading Cobalt Single Atoms. *Energy Storage Mater.* **2020**, 30, 250–259. doi.org/10.1016/j.ensm.2020.05.022.
- [41] Wan, X., Liu, X., Li, Y., Yu, R., Zheng, L., Yan, W., Wang, H., Xu, M., Shui, J. Fe–N–C Electrocatalyst with Dense Active Sites and Efficient Mass Transport for High-Performance Proton Exchange Membrane Fuel Cells. *Nat. Catal.* **2019**, 2 (3), 259–268. doi.org/10.1038/s41929-019-0237-3.
- [42] Charretier, F., Ruggeri, S., Jaouen, F., Dodelet, J. P. Increasing the Activity of Fe/N/C Catalysts in PEM Fuel Cell Cathodes Using Carbon Blacks with a High-Disordered Carbon Content. *Electrochimica Acta* **2008**, 53 (23), 6881–6889. doi.org/10.1016/j.electacta.2007.12.051.
- [43] Sougrati, M. T., Goellner, V., Schuppert, A. K., Stievano, L., Jaouen, F. Probing Active Sites in Iron-Based Catalysts for Oxygen Electro-Reduction: A Temperature-Dependent 57Fe Mössbauer Spectroscopy Study. *Electrocatalysis* **2016**, 262, 110–120. doi.org/10.1016/j.cattod.2015.10.017.
- [44] Mineva, T., Matanovic, I., Atanassov, P., Sougrati, M.-T., Stievano, L., Clémancey, M., Kochem, A., Latour, J.-M., Jaouen, F. Understanding Active Sites in Pyrolyzed Fe–N–C Catalysts for Fuel Cell Cathodes by Bridging Density Functional Theory Calculations and 57Fe Mössbauer Spectroscopy. *ACS Catal.* **2019**, 9 (10), 9359–9371. doi.org/10.1021/acscatal.9b02586.
- [45] Wu, N., Wang, Y., Lei, Y., Wang, B., Han, C., Gou, Y., Shi, Q., Fang, D. Electrospun Interconnected Fe-N/C Nanofiber Networks as Efficient Electrocatalysts for Oxygen Reduction Reaction in Acidic Media. *Sci. Rep.* **2015**, 5 (1), 17396. doi.org/10.1038/srep17396.
- [46] Kim, J., Kim, S.-J., Jung, E., Mok, D. H., Paidi, V. K., Lee, J., Lee, H. S., Jeoun Y., Ko W., Shin H., Lee B.-H., Kim, S.-Y., Kim, H., Kim, J. H., Cho, S.-P., Lee K.-S., Back, S., Yu, S.-H., Sung, Y.-E., Hyeon, T. Atomic Structure Modification of Fe–N–C Catalysts *via* Morphology Engineering of Graphene for Enhanced Conversion Kinetics of Lithium–Sulfur Batteries. *Adv. Funct. Mater.* **2022**, 32, 2110857. doi.org/10.1002/adfm.202110857
- [47] Wenguo, W., Babu D., Yiyin, H., Lv, J., Wang, Y., Wu, M. Atomic Dispersion of Fe/Co/N on Graphene by Ball-Milling for Efficient Oxygen Evolution Reaction. *Int. J. Hydrog. Energy* **2018**, 43 (22), 10351–10358. doi.org/10.1016/j.ijhydene.2018.04.108
- [48] Li, W., Wei, D., Wu, G., Jianhua, L., Nie, Y., Xueqiang, Q., Li, L., Siguo, C., Zidong, W. Cobalt Modified Two-Dimensional Polypyrrole Synthesized in a Flat Nanoreactor for the

- Catalysis of Oxygen Reduction. *Chem Eng Sci* **2015**, *135*, 45–51. doi.org/10.1016/j.ces.2015.07.008
- [49] Sun, M., Dong, Y., Zhang, G., Qu, J., Li, J. α -Fe₂O₃ Spherical Nanocrystals Supported on CNTs as Efficient Non-Noble Electrocatalysts for the Oxygen Reduction Reaction. *J Mater Chem A* **2014**, *2*, 13635–13640. DOI:10.1039/C4TA02172J
- [50] Barchasz, C., Molton, F., Duboc, C., Leprêtre, J.-C., Patoux, S., Alloin, F. Lithium/Sulfur Cell Discharge Mechanism: An Original Approach for Intermediate Species Identification, *Anal. Chem.* **84** (2012) 3973–3980. doi.org/10.1021/ac2032244.
- [51] Nicholson, R.S. Theory and Application of Cyclic Voltammetry for Measurement of Electrode Reaction Kinetics, *Anal. Chem.* **37** (1965) 1351–1355 doi.org/10.1021/ac60230a016
- [52] Dragu, D., Buda, M., Visan, T. Cyclic Voltammetry Simulation Using Orthogonal Collocation: Comparison with Experimental Data and Measure the Electrochemical Rate Constant. *U.P.B.Sci.Bull.* **2009**, *71* (3) 77-90
- [53] Wang, Z., Li, Y., Ji, H., Zhou, J., Qian, T., Yan, C. Unity of Opposites between Soluble and Insoluble Lithium Polysulfides in Lithium–Sulfur Batteries. *Adv. Mater.* **2022**, *47* (34), 2203699. doi.org/10.1002/adma.202203699.
- [54] Wang, Y., Adekoya, D., Sun, J., Tang, T., Qiu, H., Xu, L., Zhang, S., Hou, Y. Manipulation of Edge-Site Fe–N₂ Moiety on Holey Fe, N Codoped Graphene to Promote the Cycle Stability and Rate Capacity of Li–S Batteries. *Adv. Funct. Mater.* **2019**, *29* (5), 1807485. doi.org/10.1002/adfm.201807485.
- [55] Ding, Y., Cheng, Q., Wu, J., Yan, T., Shi, Z., Wang, M.; Yang, D., Wang, P., Zhang, L., Sun, J. Enhanced Dual-Directional Sulfur Redox via a Biotemplated Single-Atomic Fe–N₂ Mediator Promises Durable Li–S Batteries. *Adv. Mater.* **2022**, *34* (28), 2202256. doi.org/10.1002/adma.202202256.
- [56] Shi, H., Su, P., Dong, C., Liu, J., Wu, Z.-S. Atomic Fe–N Doped Multi-Cavity Hollow Carbon Nanoreactor as an Efficient Electrocatalyst for Lithium-Sulfur Batteries. *Batter. Supercaps* **2022**, *5* (8), e202200154. doi.org/10.1002/batt.202200154.
- [57] Wang, Z., Shen, J., Xu, X., Yuan, J., Zuo, S., Liu, Z., Zhang, D., Liu, J. In-Situ Synthesis of Carbon-Encapsulated Atomic Cobalt as Highly Efficient Polysulfide Electrocatalysts for Highly Stable Lithium–Sulfur Batteries. *Small* **2022**, *18* (13), 2106640. doi.org/10.1002/sml.202106640.

